ACS OMEGA

http://pubs.acs.org/journal/acsodf

Article

Ab Initio Kinetics of Initial Thermal Pyrolysis of Isopropyl Propionate: A Revisited Study

Tam V.-T. Mai* and Lam K. Huynh*

Cite This: *ACS Omega* 2022, 7, 661−668

Read Online

ACCESS | Metrics & More | Article Recommendations | Supporting Information

ABSTRACT: This work reports a detailed mechanism of the initial thermal pyrolysis of isopropyl propionate, ($C_2H_5C(=O)OCH(CH_3)_2$), an important biodiesel additive/surrogate, for a wide range of T = 500−2000 K and P = 7.6−76 000 Torr. The detailed kinetic behaviors of the title reaction on the potential energy surface constructed at the CBS-QB3 level were investigated using the RRKM-based master equation (RRKM-ME) rate model, including hindered internal rotation (HIR) and tunneling corrections. It is revealed that the C_3H_6 elimination occurring via a six-centered retro-ene transition state is dominant at low temperatures, while the homolytic fission of the C−C bonds becomes more competitive at higher temperatures. The tunneling treatment is found to slightly increase the rate constant at low temperatures (e.g., ∼1.59 times at 563 K), while the HIR treatment, being important at high temperatures, decreases the rate (e.g., by 5.9 times at 2000 K). Showing a good agreement with experiments in low-temperature kinetics, the kinetic model reveals that the pressure effect should be taken into account at high temperatures. Finally, the temperature- and pressure-dependent kinetic mechanism, consisting of the calculated thermodynamic and kinetic data, is provided for further modeling and simulation of any related systems.

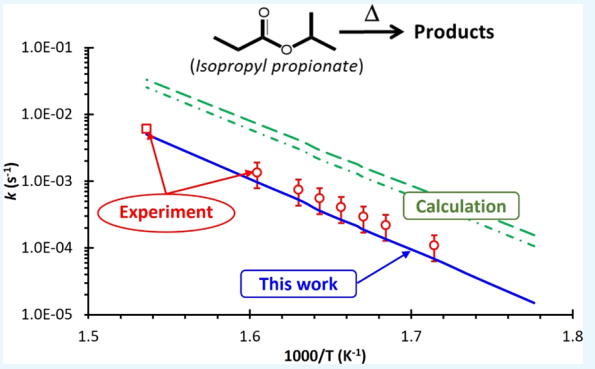

INTRODUCTION

Biodiesels, commonly composed of fatty acid alkyl esters, are typically transesterified by short-chain alcohols (e.g., methanol, ethanol, and propanol) and triglycerides (greases and plant fats).[1−7] Biodiesels can be considered as renewable fuels used in internal combustion engines due to their replacement of conventional diesel fuels.[4] However, the flow property, one of the main disadvantages of biodiesels, makes their utilization limited because it vulnerably depends on the season and region for using the fuels.[8] The property can be significantly improved with esters attained from the isopropyl or isoamyl alcohols due to the reducing intramolecular interactions at low temperatures.[9] Also, the initial reactions of the thermal pyrolysis of biofuels are important in the combustion chamber, leading to a large amount of unsaturated products and soot, which can be oxidized later.[10] Therefore, detailed studies on the thermal decomposition of biofuels for a wide range of conditions are essential for constructing a detailed kinetic model.[11]

As an essential biodiesel additive and surrogate, isopropyl propionate [IPP−$C_2H_5C(=O)OCH(CH_3)_2$] has attracted much attention to study its combustion characteristics. The kinetics of the thermal decomposition of IPP, reported by Chuchani et al.[12] in homogenous static vessels at T = 583−623 K and P ∼ 760 Torr, was found to follow the first-order law as $k(T) = 10^{(13.06\pm0.09)} \times \exp\{[-(45\,400 \pm 200)\ \text{cal mol}^{-1}]/RT\}\ \text{s}^{-1}$. The formed propene was quantitatively analyzed on gas chromatography using a thermal conductivity detector. Smith et al.[13] also reported measured value of $(6.10 \pm 0.20) \times 10^{-3}\ \text{s}^{-1}$ for the thermal pyrolysis of IPP using a static reactor at T ∼ 651 K. Theoretically, Shiroudi et al.[8] reported the calculated rate constants for the temperature range of 563−651 K. Their reported rate constants are much higher than the experimental data by an average factor of about 5.4 and 3.9 using TST/Eckart and RRKM models, respectively.

In addition to the large discrepancy in kinetics between experiments and calculations, the insights into the kinetic behaviors of the title system for a wide range of temperature and pressure, needed for the modeling and simulation of related systems, have motivated us to reinvestigate its kinetic behaviors for a broad condition range of T = 500−2000 K and P = 7.6−76 000 Torr. In particular, in this study, we used the RRKM-based master equation (RRKM-ME) rate model, including hindered internal rotation (HIR) and tunneling corrections, to investigate the kinetic behaviors on the potential energy surface constructed at the CBS-QB3 level. The derived temperature- and pressure-dependent kinetic mechanism, consisting of the calculated

Received: September 23, 2021
Accepted: November 30, 2021
Published: December 20, 2021

https://doi.org/10.1021/acsomega.1c05280
ACS Omega 2022, 7, 661−668

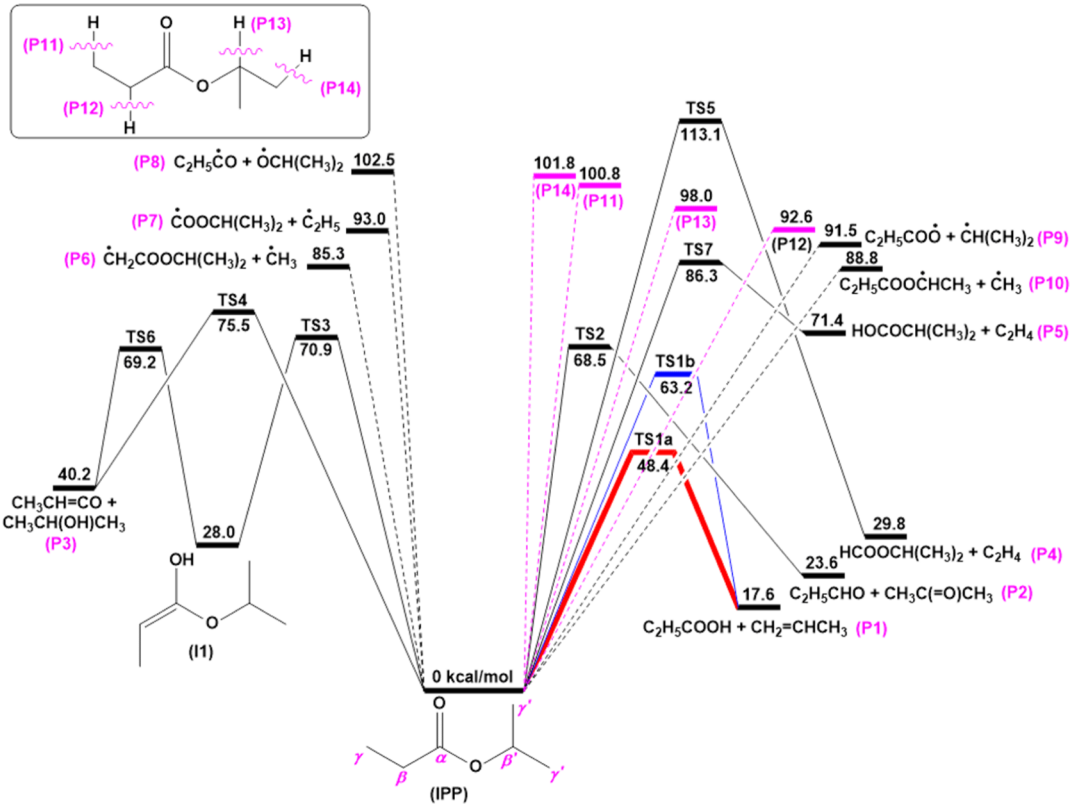

Figure 1. ZPE-corrected energy profile (0 K) for the initial thermal pyrolysis of IPP, calculated at the CBS-QB3 level with the lowest energy-lying structure for a species of interest. Units are in kcal mol^{-1}.

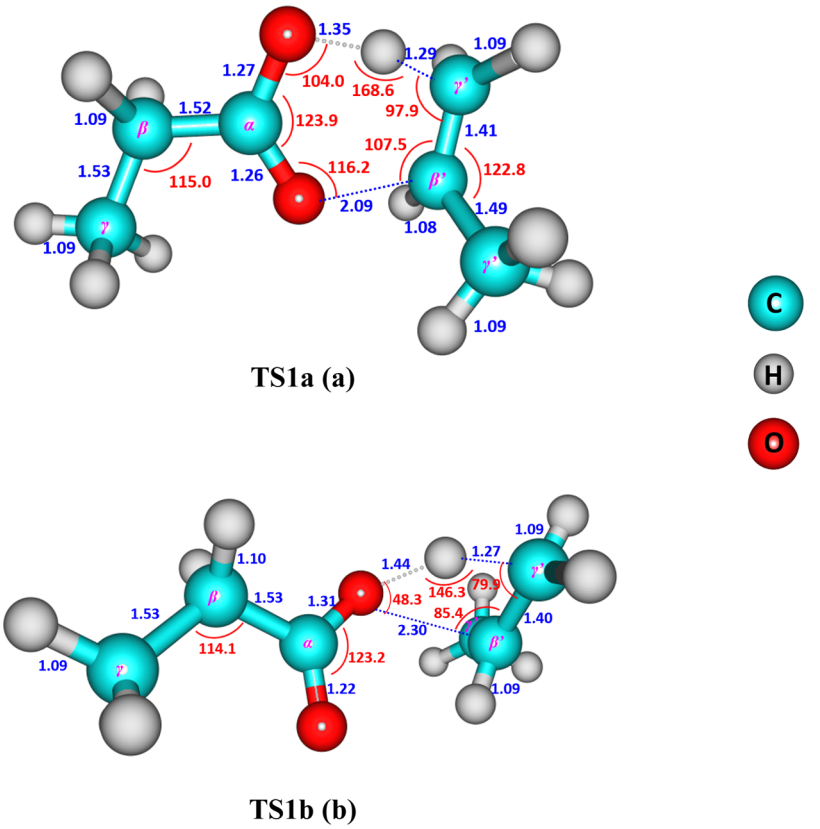

Figure 2. Optimized structures of **TS1a** (a) and **TS1b** (b) obtained at the B3LYP/CBSB7 level of theory. Bond lengths and angles are in Å and degree (°), respectively.

https://doi.org/10.1021/acsomega.1c05280
ACS Omega 2022, 7, 661−668

thermodynamic and kinetic data for main reaction channels, is also provided for further kinetic modeling and simulation of any related systems.

COMPUTATIONAL METHODOLOGY

All quantum chemical calculations were done using Gaussian 09 suite.[14] The geometry optimization and frequency calculations employ the hybrid density functional theory, namely, the B3LYP/CBSB7[15−17] level of theory. Found to be suitable for investigating the detailed kinetics of the similar reactions of methyl propionate radicals[18] /methyl acetate radicals[19] with an O_2 molecule, the composite method CBS-QB3,[20] based on the B3LYP/CBSB7 geometry, was used to obtain the energies of all species involved.

The HIR corrections were thoroughly taken into account in thermodynamic/kinetic calculations, in which the hindrance potentials of the rotation along the C−C and C−O "single" bonds were calculated at the B3LYP/CBSB7 level via relaxed surface scans (cf. Figure S8 for the details). The HIR parameters were determined using the multi-species multi-channels (MSMC) graphical user interface.[21,22] The procedure of the HIR correction calculation can be found in our previous work.[23] The Eckart tunneling correction[24] was also included in the rate constant calculations for all elementary reaction channels. The microcanonical rate constants $k(E)$ of the barrierless paths (namely, breaking the C−C and C−H bonds of IPP, cf. Figure 1) were derived from the high-pressure limit values, $k^{\infty}(T)$, of the somewhat similar system, ethyl propionate (EP)[25] (see Table S6 for the details), using the inverse Laplace transform technique.[26] For the energy transfer process, the expression of $\langle \Delta E_{down} \rangle = 250.0 \times (T/298)^{0.8}$ cm^{-1} was used for the bath gas of N_2.[27] The Lennard-Jones parameters of ε/k_B = 82.0 K and σ = 3.74 Å were adopted for N_2,[28] so then ε/k_B = 454.4 K and σ = 5.9 Å were taken for IPP and its isomer.[29] The canonical transition state (TST) theory and stochastic[30,31] /deterministic[32,33] RRKM-ME[32] rate models, including the HIR and tunneling corrections, were used for the kinetic analyses for a broader condition range of T = 500−2000 K and P = 7.6−76 000 Torr. The MSMC code,[34] an ab initio-based kinetic/thermodynamic code for complex chemical systems by solving the ME with deterministic and stochastic approaches, was used for all thermodynamic and kinetic calculations in this study.

RESULTS AND DISCUSSION

The energetic profile (0 K) for the initial thermal pyrolysis of IPP is plotted in Figure 1, calculated at the CBS-QB3 level. As seen in Figure 1, IPP is most likely decomposed in a concerted mechanism via tight six-center and four-center transition states, **TS1a** and **TS1b**, at 48.4 and 63.2 kcal mol^{-1}, respectively. The structures of the two transition states (cf. Figure 2) reveal that one H atom of the $C_{\gamma'}$−H group migrates to the O atom of C_{β}═O and C_{β}−O moieties, respectively, associated with the spontaneous breaking of the C_{β}−O bond to form the same products, $C_2H_5COOH + C_3H_6$ (**P1**), at 17.6 kcal mol^{-1}. From a kinetic point of view, the **TS1a**-via channel is expected to be the most favorable due to its lowest barrier height of 48.4 kcal mol^{-1} at 0 K, comparable with those of ethyl acetate (EA) (49.5 kcal mol^{-1})[35] and EP (48.9 kcal mol^{-1}).[36] This expectation is confirmed later in the kinetic analysis, which includes the enthalpic and entropic effects in the considered T and P range. The **TS1a**-via barrier height was also calculated at a higher level, CCSD(T)/cc-pVTZ//B3LYP/aug-cc-pVTZ,[37−39] and an excellent agreement between the two methods is observed (48.4 vs 48.2 kcal mol^{-1}); thus, the CBS-QB3 can be reasonably considered as the method of choice for this system, at least for this important channel. It is worth noting that **TS1b**, not reported previously, is energetically consistent with the similar channels observed in ethyl 2-furoate and EP (63.2 vs 63.7[40] and 65.5[36] kcal mol^{-1}, respectively) systems. Because of the higher barrier (compared to **TS1a**), this reaction channel is believed not to be crucial at low temperatures (e.g., the range of 563−651 K covered by the previous experiments[12,13]), but it is expected to play a role at high temperatures (see the kinetic analysis below).

In addition to the **P1** formation via **TS1a** and **TS1b**, IPP can be decomposed by the cleavage of C_{α}−O and $C_{\beta'}$−H bonds (see Figure 1 for the notations) via the transition state **TS2** at 68.2 kcal mol^{-1}, which leads to the formation of $C_2H_5CHO + CH_3C(=O)CH_3$ (**P2**), located 23.6 kcal mol^{-1} above the reactant. IPP can also isomerize to form the enol intermediate, **I1**, through **TS3**, followed by the unimolecular dissociation **TS6**-via reaction, leading to the final products, $CH_3CHCHO + CH_3CH(OH)CH_3$ (**P3**). It is found that **I1** is at 28.0 kcal mol^{-1} above the entrance channel, and **TS3** and **TS6** have barriers of 70.9 and 41.2 kcal mol^{-1}, respectively, which are reasonably comparable with those of EA,[35] for example, 70.6 and 42.6 kcal mol^{-1}, respectively. On the other hand, IPP can directly dissociate to **P3** via **TS4** with a 75.5 kcal mol^{-1} barrier, slightly higher than EA[35] (72.9 kcal mol^{-1}). The C_2H_4 elimination channels via **TS5** and **TS7** proceed with high barriers of 113.1 and 86.3 kcal mol^{-1}, respectively, leading to products $HCOOCH(CH_3)_2 + C_2H_4$ (**P4**) and $HOCOCH(CH_3)_2 + C_2H_4$ (**P5**), respectively, but the latter channel is found less thermodynamically favorable at 0 K (i.e., 71.4 vs 29.8 kcal mol^{-1}, respectively). It could be expected that these channels via the C_2H_4-elimination mechanism could hardly play a role from the kinetic point of view due to their high barrier heights.

Moreover, IPP can be thermally decomposed by breaking the C−C bonds via typical barrierless pathways to yield the two radical fragments, namely, $^{\bullet}CH_2COOCH(CH_3)_2 + {}^{\bullet}CH_3$ (**P6**), $^{\bullet}COOCH(CH_3)_2 + {}^{\bullet}C_2H_5$ (**P7**), $C_2H_5C^{\bullet}O + {}^{\bullet}OCH(CH_3)_2$ (**P8**), $C_2H_5COO^{\bullet} + {}^{\bullet}CH(CH_3)_2$ (**P9**), and $C_2H_5COOC^{\bullet}HCH_3 + CH_3$ (**P10**) with the high barriers of 85.3, 93.0, 102.5, 91.5, and 88.8 kcal mol^{-1}, respectively. Similarly, IPP can also experience the unimolecular dissociations via cracking the C−H bonds without an intrinsic barrier height, leading to the final products $^{\bullet}CH_2CH_2COOCH(CH_3)_2 + H^{\bullet}$ (**P11**), $CH_3C^{\bullet}HCOOCH(CH_3)_2 + H^{\bullet}$ (**P12**), $C_2H_5COOC^{\bullet}(CH_3)_2 + H^{\bullet}$ (**P13**), and $C_2H_5COOCH(CH_3)$-$C^{\bullet}H_2 + H^{\bullet}$ (**P14**) with the reaction enthalpy of 100.8, 92.6, 98.0, and 101.8 kcal mol^{-1}, respectively. In short, these homolytic bond cleavage reactions are not favorable at low temperatures (e.g., $T \leq$ 1000 K), but they could become significant at high temperatures (e.g., $T >$ 1500 K).

Compared to the numbers previously suggested at the same level of theory, our calculated numbers consistently match those reported by Shiroudi et al.[8] with the mean absolute deviation (MAD) value of 0.24 kcal mol^{-1} between the two data sets (cf. Table S2). The calculated thermodynamic properties (ΔH_f^{298K} and S^{298K}) for all species involved in the title reaction were also tabulated in Table S4, and those fitted to the NASA format are provided in Table S3. Comparison with the literature data (i.e., those from the NIST and ATcT databases) was carried out to evaluate the accuracy of the derived numbers at the CBS-QB3[41] level of theory. Our calculated ΔH_f^{298K} and S^{298K} consistently match those obtained from NIST and ATcT databases for

https://doi.org/10.1021/acsomega.1c05280
ACS Omega 2022, 7, 661−668

several available species (e.g., the MAD values are 0.6 and 0.8 kcal mol^{-1} for ΔH_f^{298K}, and 0.2 and 1.3 cal mol^{-1} K^{-1} for S^{298K}, respectively).

Figure 3 representatively shows the normalized time-resolved profiles for the IPP → products reaction (at 760 Torr) at two

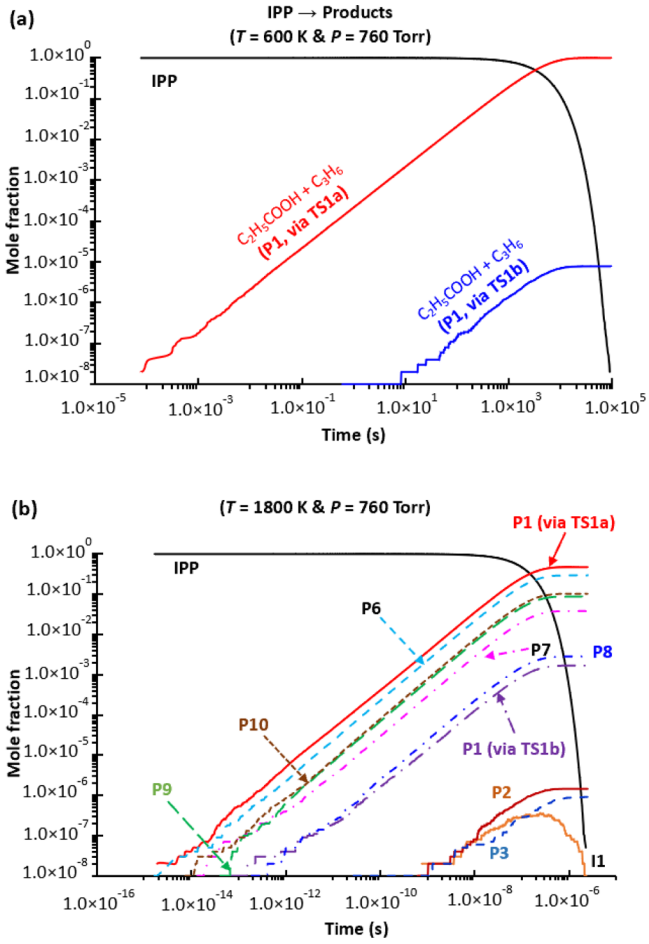

Figure 3. Time-resolved species profiles for the reaction of IPP → products, calculated at P = 760 Torr (in the logarithm scale) using the stochastic (solid lines, 10^8 trials) model at two temperatures: T = 600 K (a) and T = 1800 K (b). The simulations were performed using the full PES represented in Figure 1. Species notations are provided in Figure 1. X-/Y-axes are in the base-10 logarithm scale.

temperatures, 600 and 1800 K, using the stochastic[30,31] RRKM-ME rate models. It is observed that the mechanism changes with temperature. At the low temperature, the formation of C_2H_5COOH + C_3H_6 (**P1**) via **TS1a** and **TS1b** is the major and minor pathways, respectively (e.g., the former is about 5 orders of magnitude faster than the latter). Note that the contribution of the other channels is too small to appear in Figure 3a. It is worth noting that the stochastic[30,31] and deterministic[32,33] models predict the same time-resolved species profiles (cf. Figure S2) and the same overall rate constant, k_{tot}, (cf. Figure S3, with the MAD value of 12.9%) for the IPP → products reaction for a wide range of temperature of 500−2000 K and P = 760 Torr. Therefore, the two models can independently be used to quantify the chemical behaviors reliably for the title reaction. At the high temperature of 1800 K, the main reaction channels, in the decreasing order, are **P1** (via **TS1a**), **P6**, **P9** ∼ **P10**, **P7**, **P8**, **P1** (via **TS1b**), **P2,** and **P3**. Note that the profile of intermediate **I1**, with the mole fraction of ∼10^{-6}, also appears in Figure 3b.

Our predicted rate constants, $k(T, P = 760\ K)$, for the IPP → products reaction (shown in Figure 4 and the discrete calculated values are provided in Table 1) are in much better agreement with the measured data[12,13] than those reported by Shiroudi et al.[8] For instance, at T = 583 K, we report the value of 6.7 × 10^{-5}, which is very close to the experimental value of 10.9 × 10^{-5} by Chuchani et al.,[12] while Shiroudi et al.[8] suggested the much higher values of 61.7 × 10^{-5} and 43.6 × 10^{-5} s^{-1} (using the TST/Eckart and RRKM models, respectively). At T = 651 K, the numbers are 5.0 × 10^{-3} s^{-1} (this work), 6.1 × 10^{-3} s^{-1} (experimental number by Smith et al.[13]), and 33.2 × 10^{-3} and 25.3 × 10^{-3} s^{-1} (Shiroudi et al.,[8] using the TST/Eckart and RRKM models, respectively). Note that the data for a wider temperature and pressure range (i.e., T = 500−2000 K and P = 7.6−76 000 Torr) are presented in Figure 5. The calculated kinetic data using two different models (i.e., TST and RRKM-ME), including the corrections of HIR and Eckart tunneling treatments at T = 563−651 K and P = 760 Torr, are also presented in Table 1. It is observed that at atmospheric pressure, the rate constants reach their high-pressure limit values [i.e., k(RRKM/ME) ≈ k(TST)], which is somehow consistent with the data reported by Shiroudi et al. [e.g., k(RRKM) = ∼76% k(TST) at T = 651 K] in the same condition. The difference of the high-pressure value $k(P = \infty)$ and the pressure-dependent rate constant $k(P$ = 760 Torr) between the two models [i.e., between our observation of "k(RRKM/ME) ≈ k(TST)" and the reported "k(RRKM) = ∼76% k(TST)" by Shiroudi et al.] is likely due to different pressure-dependent kinetic models used in the two studies.

To learn more about the difference between our numbers and those suggested by Shiroudi et al.,[8] we compared the high-pressure rate constants ($k^{\infty}(T)$) calculated using two similar kinetic models. In particular, the TST rate models, together with the Eckart tunneling correction, on the potential energy surfaced explored at the CBS-QB3 level were used with two different kinetic codes, our MSMC code and KiSThelP[20] code by Shiroudi et al.[8] There is a large difference of an average factor of ∼5 (e.g., 6.65 and 4.04 at 563 and 651 K, respectively, cf. Figure 4) between our numbers and those reported by Shiroudi and coworkers. We think such a difference is very likely due to a mistake or different parameters used in the previous calculations, and resolving this issue, which certainly is informative but not so significant, might take us a lot of time and effort that exceeds the scope of this study. It is worth noting that our calculated numbers are in excellent agreement with the experimental data without adjusting any parameters.

To understand the thermodynamic insights into the **TS1a**-via channel, the Gibbs free energy differences ($\Delta G^{\ddagger}$), together with the enthalpic ($\Delta H^{\ddagger}$) and entropic ($-T \times \Delta S^{\ddagger}$) contributions, between the transition state **TS1a** and the reactant (IPP) for the temperature range of 500−2000 K are calculated and provided in Table S5. It can be seen that the enthalpic component determines the magnitude and the sign of $\Delta G^{\ddagger}$, favoring the **TS1a** formation with the temperature increase (i.e., $\frac{[TS1a]_{eq}}{[IPP]_{eq}} = \exp\left[-\frac{\Delta G^{\ddagger}(T)}{RT}\right]$ increases with temperature). The negative values of the entropic component ($-T \times \Delta S^{\ddagger}$), having the maximum magnitude at around 1200−1300 K, suggest the **TS1a** formation is not favorable entropically as expected as the transition state with the six-membered ring structure (cf. Figure 2) reduces the degrees of freedom of the reactant. On the other

https://doi.org/10.1021/acsomega.1c05280
ACS Omega 2022, 7, 661−668

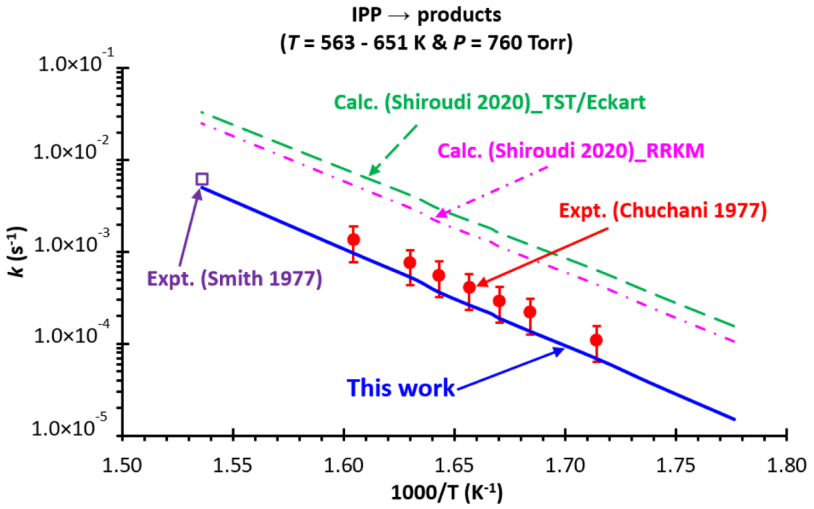

Figure 4. Comparison of the rate constants for the reaction of IPP → products, derived from this work and the literature at P = 760 Torr and T = 563−651 K. The literature data were reported by Smith et al. ["Expt. (Smith 1977)"];[13] Chuchani et al. ["Expt. (Chuchani 1977)"];[12] and Shiroudi et al. ["Calc. (Shiroudi 2020)"].[8] The predictions were performed using the full PES represented in Figure 1. The Y-axis is in the base-10 logarithm scale.

Table 1. Rate Constants (k, unit: s^{-1}), HIR Factors (f_{HIR}) and Eckart Factors (κ) for the Main Channel, IPP → CH_3CH_2COOH + CH_2CHCH_3 (via TS1a) at T = 563−651 K and P = 760 Torr, Calculated at the CBS-QB3 Method[b]

T (K)	this work				Expt'l k	
	k(TST)[a]	k(RRKM/ME)[a]	f_{HIR}	κ	Chuchani[12]	Smith[13]
563	1.51×10^{-5}	1.51×10^{-5}	0.65	1.59		
575	3.69×10^{-5}	3.69×10^{-5}	0.64	1.56		
583	6.71×10^{-5}	6.71×10^{-5}	0.64	1.54	1.09×10^{-4}	
594	1.39×10^{-4}	1.39×10^{-4}	0.63	1.51	2.20×10^{-4}	
599	1.94×10^{-4}	1.94×10^{-4}	0.63	1.50	2.95×10^{-4}	
600	2.12×10^{-4}	2.12×10^{-4}	0.63	1.50		
604	2.70×10^{-4}	2.70×10^{-4}	0.63	1.49	4.07×10^{-4}	
609	3.73×10^{-4}	3.73×10^{-4}	0.63	1.48	5.53×10^{-4}	
613	5.14×10^{-4}	5.14×10^{-4}	0.62	1.47	7.44×10^{-4}	
623	9.55×10^{-4}	9.55×10^{-4}	0.62	1.45	1.35×10^{-3}	
651	5.01×10^{-3}	5.00×10^{-3}	0.61	1.41		6.20×10^{-3}

[a]Corrections for the HIR and Eckart tunneling treatments were included. [b]RRKM model with strong collision approximation at 760 Torr.

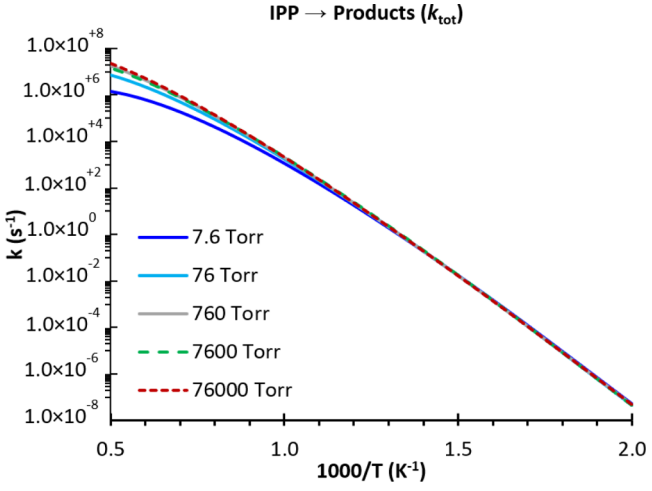

Figure 5. Computed total rate coefficients, $k_{tot}(T, P)$, for the IPP → products reaction as a function of temperature at different pressures (i.e., 7.6, 76, 760, 7600, and 7600 Torr).

hand, the thermodynamic driving force of the IPP → C_3H_6 + C_2H_5COOH (**P1**) reaction is controlled by the entropic effect ($-T \times \Delta_{rxn}S$), not the enthalpic one ($\Delta_{rxn}H$), which also favors the formation of product **P1** with temperature.

Also, within the simple Arrhenius expression $k(T) = A \times \exp(-E_a/(RT))$, the pre-exponential A-factor and activation E_a values depend on the temperature range in which the expression is derived. Note that A-factor and E_a values serve as fitting parameters, which do not account for the curvature of the plots. The fitting expressions at P = 760 Torr for two different temperature ranges of 563−651 K (covered by the experiments) and 500−2000 K are as follows

$$k(T) = (6.79 \times 10^{13}\ s^{-1}) \times \exp(-48.1\ \text{kcal mol}^{-1}/(RT))$$

for T = 563−651 K (fitting error = 0.6%)

$$k(T) = (1.51 \times 10^{12}\ s^{-1}) \times \exp(-42.5\ \text{kcal mol}^{-1}/(RT))$$

for T = 500−2000 K (fitting error = 39.2%)

It can be seen that in the same temperature range of T = 563−651 K, our model predicts higher A-factor (~5.9 times) and E_a (~2.7 kcal mol^{-1}) values when compared with experimental values reported by Chuchani et al. (1977)[12] [$k(T) = (1.15 \times 10^{13}\ s^{-1}) \times \exp(-45.4\ \text{kcal mol}^{-1}/(RT))$]. Higher A-factor and E_a values make the rate constants faster and slower, respectively;

https://doi.org/10.1021/acsomega.1c05280
ACS Omega 2022, 7, 661−668

thus, the combination of the two effects results in a good agreement between our numbers and experimental values (e.g., 6.7×10^{-5} compared with the experimental value of 10.9×10^{-5} by Chuchani et al.[12] at T = 583 K). Note that an A-factor value depends on the partition function ratio (including corrections for the tunneling and HIR treatments) of the corresponding transition state to the reactants for a chemical reaction.

Furthermore, analysis shows that the tunneling treatment slightly increases the rate constant at low temperatures. For example, the rate constants of the most dominant channel (via **TS1a**) are increased by a factor of 1.59 and 1.41 at T = 563 and 651 K, respectively (cf. Table 1), which is consistent with that predicted by Shiroudi et al.[8] (e.g., 1.41 and 1.31 at T = 563 and 651 K, respectively). In contrast, the HIR treatment, which is not taken into account by Shiroudi et al.,[8] decreases the rate constants of the **TS1a**-via channel by a factor of 0.65 and 0.61 at T = 563 and 651 K, respectively, at P = 760 Torr (cf. Table 1). It is found that the HIR treatment still plays a role at high temperatures, for example, it decreases the total rate constants, k_{tot}, by a factor of 0.70 and 0.17 at 500 and 2000 K, respectively, at P = 760 Torr (cf. Figure S6). As also seen in Figure S7, our calculated rate constant of IPP → P1 reaction is notably lower than that of Shiroudi et al.,[8] for example, 6.1 and 52.0 times at 600 and 2000 K, respectively, at P = 760 Torr. Also, even though the two corrections relatively compensate each other in the rate constants at the low experimental temperatures, the inclusion of both tunneling (necessary at low temperatures) and HIR (important at high temperatures) treatments is pivotal in determining the reliable rate constants for the initial thermal decomposition of IPP for the wide range of T and P conditions as in this study.

The species branching ratios from the reactants, representatively at P = 760 Torr as a function of temperatures, are illustrated in Figure S7. It is observed that the **P1** formation is the only main channel until 1600 K and then decreases until 2000 *K*, where the **P6** channel becomes comparable and other channels (e.g., **P7**, **P10,** and **P9**) are observable. It is noteworthy that experimentally Giri et al.[36] only found the formation of propionic acid and ethylene via a six-centered retro-ene transition state for the thermal pyrolysis of EP at T = 976−1300 K and P = 825−1875 Torr, while Shiroudi and coworkers[8] observed that the so-called similar **P1** channel dominates in a lower temperature range (i.e., T < 1200 K). In other words, the breaking of the C−C bonds (i.e., channels **P6**, **P7**, **P9,** and **P10**) was found significant by Shiroudi et al. at T > 1200 K, while it is expected that the two similar systems should behave similarly in the same high-temperature domain. According to our model, the homolytic fission of the C−C bonds becomes significantly substantial (i.e., **P6** > **P7** > **P9** ∼ **P10**) at high temperature while the homolytic bond breakage of the C−H bonds still cannot compete due to their high bonding dissociation energies (e.g., >92.6 kcal mol^{-1}, cf. Figure 1). It is recommended that a detailed laboratory study should be conducted at combustion-relevant conditions (i.e., $T \geq$ 1000 K) to confirm the branching ratios reported here.

Computed rate coefficients, $k(T, P)$, for the IPP → products reaction as a function of temperature at different pressures are plotted in Figure 5. Because the plots are for the total rate constants of the title reaction (not an elementary reaction), the curvatures of the plots, which are higher at lower temperatures and pressures, depend on many factors, including the temperature-dependent tunneling and HIR corrections and temperature and pressure. It is observed that the pressure effect is only noticeable at the high temperatures [e.g., T > 1000 K, $k(P$ = infinity$)/k(P$ = 7.6 Torr) = ∼6 at T = 1500 K]; thus, the pressure effect should be taken into account for the pyrolysis at low pressures and high temperatures, causing the changes in the rate constants and species branching ratios in such conditions. Also, the **TS1b**-via channel plays a minor role in the temperature range of 563−651 K covered by the previous experiments[12,13] and becomes observable in the high-temperature regime (e.g., at $T \geq$ 1500 K and $P = \infty$, cf. Figure S5);[40] thus, together with the homolytic bond cleavage reactions, it is recommended to be included in the pyrolysis mechanism for the title reaction. For the overall decomposition of IPP, the total rate constants (in the modified Arrhenius expression) of the title reaction at different pressures are given in Table 2. Also, the thermodynamically consistent kinetic submechanism, which consist of $k(T, P)$ of the important channels, that is, those forming **P1**, **P6**, **P7**, **P8**, **P9,** and **P10** (cf. Table S7) and the thermodynamic data of the species involved (cf. Table S3), is provided for T = 500−2000 K and P = 7.6−7600 Torr to describe the kinetic behaviors (including the rate constants and branching ratios) of the title reaction. Such a kinetic submechanism could be incorporated into an extended kinetic mechanism to construct a full detailed kinetic model for further modeling IPP-related systems for a wide range of conditions.

Table 2. Kinetic Parameters of the Modified Arrhenius Expression (K_{tot}) for the Thermal Decomposition of IPP → Products Reaction at Different Pressures at T = 500−2000 K

P (Torr)	A (s^{-1})	n	E_a/R (K)	fitting uncertainty (%)
7.6	9.51×10^{58}	−13.81	3.34×10^4	6.3
76	5.96×10^{50}	−10.19	3.21×10^4	7.7
760	4.06×10^{43}	−9.00	3.06×10^4	0.2
7600	2.38×10^{47}	−10.11	3.16×10^4	7.4
76 000	1.36×10^{42}	−8.54	3.04×10^4	0.2

CONCLUSIONS

In conclusion, the kinetic behaviors of the title reaction were investigated for a wide range of conditions (T = 500−2000 K and P = 7.6−76 000 Torr) using the RRKM-ME rate model, which includes the HIR and tunneling corrections, on the comprehensive PES constructed at the CBS-QB3 level. The mechanistic insights were revealed as the C_3H_6 elimination occurring via a six-centered retro-ene transition state is dominant at low temperatures and the homolytic fission of the C−C bonds becomes noticeable at higher temperatures. Showing a good agreement in the rate constants with experiments at low temperatures, the models suggest that the pressure effect should only be considered at high temperatures and low pressures. Moreover, this work provides the detailed kinetic mechanism, consisting of thermodynamic (in the NASA format) and kinetic (in the modified Arrhenius format) data for main reaction channels at different conditions, for further modeling/simulation of biodiesel-related combustion systems.

ASSOCIATED CONTENT

Supporting Information

The Supporting Information is available free of charge at https://pubs.acs.org/doi/10.1021/acsomega.1c05280.

Optimized geometries, electronic energies at 0 K, ZPE corrections and harmonic wavenumbers of the species involved in the title reaction, calculated at the CBS-QB3

https://doi.org/10.1021/acsomega.1c05280
ACS Omega 2022, 7, 661−668

level of theory; comparison of the relative ZPE-corrected energies of all species, calculated at the same method, CBS-QB3; calculated thermodynamic data (in the NASA format) of all species; comparison of predicted thermochemical properties of all species with the literature data; Gibbs free energy differences (ΔG) and their corresponding enthalpic (ΔH) and entropic ($-T \times \Delta S$) components for the **TS1a**-via IPP → C_3H_6 + C_2H_5COOH (**P1**) reaction in the temperature range of 500−2000 K; estimated high-pressure limited rate constants, $k^{\infty}(T)$, for the barrierless channels of IPP in the considered temperature range of 500−2000 K; predicted rate constant (1/s) of important channels from IPP (i.e., **P1**, **P6**, **P7**, **P8**, **P9**, and **P10** via channels) at different pressures (7.6−76 000 Torr); geometrical structures of all species, optimized at the B3LYP/CBSB7 level of theory; time-resolved species profiles for the reaction of IPP → products, calculated at T = 600 K and P = 760 Torr using both stochastic and deterministic RRKM-ME rate models; comparison of the calculated total rate constants, k_{tot}, for the IPP → products reaction between the stochastic and deterministic rate models as a function of temperature (T = 500−2000 K) at P = 760 Torr; calculated rate coefficients for the IPP → products reaction, at P = 760 Torr; calculated branching ratios for the reaction of IPP → CH_3CH_2COOH + CH_2CHCH_3 (**P1**) via **TS1a** and **TS1b** at T = 500−2000 K and P = 760 Torr and high-P limit (HPL); calculated rate constants for the IPP → products reaction with and without HIR treatment; calculated species branching ratios for the reaction of IPP → products as a function of temperature at P = 760 Torr; and hindrance potentials for the species involved, calculated at the B3LYP/CBSB7 level of theory (PDF)

AUTHOR INFORMATION

Corresponding Authors

Tam V.-T. Mai − *Molecular Science and Nano-Materials Lab, Institute for Computational Science and Technology, SBI Building, Quang Trung Software City, Ho Chi Minh City 70000, Vietnam; University of Science, Ho Chi Minh City 70000, Vietnam; Vietnam National University, Ho Chi Minh City 70000, Vietnam*; Email: tam.mvt@icst.org.vn

Lam K. Huynh − *Vietnam National University, Ho Chi Minh City 70000, Vietnam; International University, Ho Chi Minh City 70000, Vietnam*; orcid.org/0000-0002-3683-2787; Email: hklam@hcmiu.edu.vn

Complete contact information is available at: https://pubs.acs.org/10.1021/acsomega.1c05280

Notes

The authors declare no competing financial interest.

ACKNOWLEDGMENTS

Financial support and computational facilities are provided by the Institute for Computational Science and Technology (ICST)−Ho Chi Minh City (grant no. 454/QĐ-KHCNTT) and the Department of Science and Technology (DOST)−Ho Chi Minh City. T.V.-T.M. was funded by Vingroup Joint Stock Company and supported by the Domestic Master/Ph.D. Scholarship Programme of the Vingroup Innovation Foundation (VINIF), Vingroup Big Data Institute (VINBIGDATA) (VINIF.2020.TS.96). We would like to thank Tuyn Phan and Tri Pham (ICST) for their technical assistance.

REFERENCES

(1) Bozbas, K. Biodiesel as an alternative motor fuel: Production and policies in the European Union. *Renewable Sustainable Energy Rev.* **2008**, *12*, 542−552.

(2) Demirbas, A. Biodiesel production from vegetable oils via catalytic and non-catalytic supercritical methanol transesterification methods. *Prog. Energy Combust. Sci.* **2005**, *31*, 466−487.

(3) Graboski, M. S.; McCormick, R. L. Combustion of fat and vegetable oil derived fuels in diesel engines. *Prog. Energy Combust. Sci.* **1998**, *24*, 125−164.

(4) Agarwal, A. K. Biofuels (alcohols and biodiesel) applications as fuels for internal combustion engines. *Prog. Energy Combust. Sci.* **2007**, *33*, 233−271.

(5) Kohse-Höinghaus, K.; Osswald, P.; Cool, T. A.; Kasper, T.; Hansen, N.; Qi, F.; Westbrook, C. K.; Westmoreland, P. R. Biofuel combustion chemistry: from ethanol to biodiesel. *Angew. Chem., Int. Ed. Engl.* **2010**, *49*, 3572−3597.

(6) Madiwale, S.; Karthikeyan, A.; Bhojwani, V. A Comprehensive Review of Effect of Biodiesel Additives on Properties, Performance, and Emission. *Mater. Sci. Eng.* **2017**, *197*, 012015.

(7) Arjanggi, R. D.; Kansedo, J. Recent advancement and prospective of waste plastics as biodiesel additives: A review. *J. Energy Inst.* **2020**, *93*, 934−952.

(8) Shiroudi, A.; Hirao, K.; Yoshizawa, K.; Altarawneh, M.; Abdel-Rahman, M. A.; El-Meligy, A. B.; El-Nahas, A. M. A computational study on the kinetics of pyrolysis of isopropyl propionate as a biodiesel model: DFT and ab initio investigation. *Fuel* **2020**, *281*, 118798.

(9) Cardoso, C. C.; Mendes, B. M. O.; Pasa, V. M. D. Production and characterization of cold-flow quality biofuel from soybean oil using different alkyl and benzyl alcohols. *J. Environ. Chem. Eng.* **2018**, *6*, 2241−2247.

(10) Herbinet, O.; Glaude, P.-A.; Warth, V.; Battin-Leclerc, F. Experimental and modeling study of the thermal decomposition of methyl decanoate. *Combust. Flame* **2011**, *158*, 1288−1300.

(11) Musculus, M.; Dec, J.; Tree, D. Effects of Fuel Parameters and Diffusion Flame Lift-Off on Soot Formation in a Heavy-Duty DI Diesel Engine. *SAE Technical Paper 2002-01-0889*, 2002.

(12) Chuchani, G.; Martín, I.; Yépez, M.; Díaz, M. J. Kinetics of the gas-phase pyrolysis of some secondary acetates. *React. Kinet. Catal. Lett.* **1977**, *6*, 449−454.

(13) Smith, G. G.; Mutter, L.; Todd, G. P. Steric effects in homogeneous gas-phase reactions. Pyrolysis of isopropyl esters. *J. Org. Chem.* **1977**, *42*, 44−47.

(14) Frisch, M. J.; Trucks, G. W.; Schlegel, H. B.; Scuseria, G. E.; Robb, M. A.; Cheeseman, J. R.; Scalmani, G.; Barone, V.; Mennucci, B.; Petersson, G. A.; et al. *Gaussian 09*, Revision A.1; Gaussian, Inc.: Wallingford CT, 2009.

(15) Lee, C.; Yang, W.; Parr, R. G. Development of the Colle-Salvetti correlation-energy formula into a functional of the electron density. *Phys. Rev. B: Condens. Matter Mater. Phys.* **1988**, *37*, 785−789.

(16) Becke, A. D. Density-functional thermochemistry. III. The role of exact exchange. *J. Chem. Phys.* **1993**, *98*, 5648−5652.

(17) Frisch, M. J.; Pople, J. A.; Binkley, J. S. Self-consistent molecular orbital methods 25. Supplementary functions for Gaussian basis sets. *J. Chem. Phys.* **1984**, *80*, 3265−3269.

(18) Le, X. T.; Mai, T. V. T.; Ratkiewicz, A.; Huynh, L. K. Mechanism and kinetics of low-temperature oxidation of a biodiesel surrogate: methyl propanoate radicals with oxygen molecule. *J. Phys. Chem. A* **2015**, *119*, 3689−3703.

(19) Mai, T. V.-T.; Le, X. T.; Huynh, L. K. Mechanism and kinetics of low-temperature oxidation of a biodiesel surrogate−methyl acetate radicals with molecular oxygen. *Struct. Chem.* **2014**, *26*, 431−444.

(20) Montgomery, J. A.; Frisch, M. J.; Ochterski, J. W.; Petersson, G. A. A complete basis set model chemistry. VI. Use of density functional geometries and frequencies. *J. Chem. Phys.* **1999**, *110*, 2822−2827.

(21) Le, T. H. M.; Do, S. T.; Huynh, L. K. Algorithm for auto-generation of hindered internal rotation parameters for complex chemical systems. *Comput. Theor. Chem.* **2017**, *1100*, 61−69.
(22) Le, T. H. M.; Tran, T. T.; Huynh, L. K. Identification of hindered internal rotational mode for complex chemical species: A data mining approach with multivariate logistic regression model. *Chemom. Intell. Lab. Syst.* **2018**, *172*, 10−16.
(23) Mai, T. V.-T.; Duong, M. v.; Le, X. T.; Huynh, L. K.; Ratkiewicz, A. Direct ab initio dynamics calculations of thermal rate constants for the $CH_4 + O_2 = CH_3 + HO_2$ reaction. *Struct. Chem.* **2014**, *25*, 1495−1503.
(24) Eckart, C. The Penetration of a Potential Barrier by Electrons. *Phys. Rev.* **1930**, *35*, 1303−1309.
(25) Metcalfe, W. K.; Dooley, S.; Curran, H. J.; Simmie, J. M.; El-Nahas, A. M.; Navarro, M. V. Experimental and modeling study of C5H10O2 ethyl and methyl esters. *J. Phys. Chem. A* **2007**, *111*, 4001−4014.
(26) Robertson, S. H.; Pilling, M. J.; Baulch, D. L.; Green, N. J. B. Fitting of pressure-dependent kinetic rate data by master equation/inverse Laplace transform analysis. *J. Phys. Chem.* **1995**, *99*, 13452−13460.
(27) Tan, T.; Yang, X.; Ju, Y.; Carter, E. A. Ab Initio Reaction Kinetics of $CH_3OC^*(=O)$ and $^*CH_2OC(=O)H$ Radicals. *J. Phys. Chem. B* **2016**, *120*, 1590−1600.
(28) Hippler, H.; Troe, J.; Wendelken, H. J. Collisional deactivation of vibrationally highly excited polyatomic molecules. II. Direct observations for excited toluene. *J. Chem. Phys.* **1983**, *78*, 6709.
(29) Kee, R. J.; Rupley, F. M.; Miller, J. A.; Coltrin, M. E.; Grcar, J. F.; Meeks, E.; Moffat, H. K.; Lutz, A. E.; Dixon-Lewis, G.; Smooke, M. D.; et al. *Chemkin*; Reaction Design; California, San Diego, 2010.
(30) Gillespie, D. T. A general method for numerically simulating the stochastic time evolution of coupled chemical reactions. *J. Comput. Phys.* **1976**, *22*, 403−434.
(31) Gillespie, D. T.; Hellander, A.; Petzold, L. R. Perspective: Stochastic algorithms for chemical kinetics. *J. Chem. Phys.* **2013**, *138*, 170901−170914.
(32) Miller, J. A.; Klippenstein, S. J. Master equation methods in gas phase chemical kinetics. *J. Phys. Chem. A* **2006**, *110*, 10528−10544.
(33) Robertson, S. H.; Pilling, M. J.; Jitariu, L. C.; Hillier, I. H. Master equation methods for multiple well systems: application to the 1-,2-pentyl system. *Phys. Chem. Chem. Phys.* **2007**, *9*, 4085−4097.
(34) Duong, M. v.; Nguyen, H. T.; Truong, N.; Le, T. N.-M.; Huynh, L. K. Multi-Species Multi-Channel (MSMC): An Ab Initio-based Parallel Thermodynamic and Kinetic Code for Complex Chemical Systems. *Int. J. Chem. Kinet.* **2015**, *47*, 564−575.
(35) Sun, W.; Tao, T.; Zhang, R.; Liao, H.; Huang, C.; Zhang, F.; Zhang, X.; Zhang, Y.; Yang, B. Experimental and modeling efforts towards a better understanding of the high-temperature combustion kinetics of C 3 C 5 ethyl esters. *Combust. Flame* **2017**, *185*, 173−187.
(36) Giri, B. R.; AlAbbad, M.; Farooq, A. High-temperature unimolecular decomposition of ethyl propionate. *Chem. Phys. Lett.* **2016**, *664*, 184−190.
(37) Purvis, G. D.; Bartlett, R. J. A full coupled-cluster singles and doubles model: The inclusion of disconnected triples. *J. Chem. Phys.* **1982**, *76*, 1910−1918.
(38) Scuseria, G. E.; Janssen, C. L.; Schaefer, H. F. An efficient reformulation of the closed-shell coupled cluster single and double excitation (CCSD) equations. *J. Chem. Phys.* **1988**, *89*, 7382−7387.
(39) Scuseria, G. E.; Schaefer, H. F. Is coupled cluster singles and doubles (CCSD) more computationally intensive than quadratic configuration interaction (QCISD)? *J. Chem. Phys.* **1989**, *90*, 3700−3703.
(40) Mai, T. V. T.; Lin, K. C.; Huynh, L. K. Thermal unimolecular decomposition of ethyl 2-furoate and its reactivity toward OH radicals: A theoretical study. *Int. J. Chem. Kinet.* **2020**, *52*, 580−588.
(41) Canneaux, S.; Bohr, F.; Henon, E. KiSThelP: a program to predict thermodynamic properties and rate constants from quantum chemistry results. *J. Comput. Chem.* **2014**, *35*, 82−93.

https://doi.org/10.1021/acsomega.1c05280
ACS Omega 2022, 7, 661−668